

Quantum Tunneling of Magnetization in a Large Molecular Nanomagnet – Approaching the Mesoscale

Wolfgang Wernsdorfer¹, Monica Soler², David N. Hendrickson³, George Christou²

¹Lab. L. Néel, associé à l'UJF, CNRS, BP 166, 38042 Grenoble Cedex 9, France

²Dept. of Chemistry, Univ. of Florida, Gainesville, Florida 32611-7200, USA

³Dept. of Chemistry, Univ. of California at San Diego, La Jolla, California 92093-0358, USA

(Dated: February 7, 2020)

A Mn₃₀ molecular cluster is established to be the largest single-molecule magnet (SMM) discovered to date. Magnetization versus field measurements show coercive fields of about 0.5 T at low temperatures. Magnetization decay experiments reveal an Arrhenius behavior and temperature-independent relaxation below 0.2 K diagnostic of quantum tunneling of magnetization through the anisotropy barrier. The quantum hole digging method is used to establish resonant quantum tunneling. These results demonstrate that large molecular nanomagnets, having a volume of 15 nm³, with dimensions approaching the mesoscale can still exhibit the quantum physics of the microscale.

PACS numbers: 75.45.+j, 75.60.Ej, 75.50.Xx

The study of the interface between classical and quantum physics has always been a fascinating area, but its importance has nevertheless grown dramatically with the current explosive thrusts in nanoscience. Taking devices to the limit of miniaturization (the mesoscale and beyond) where quantum effects become important makes it essential to understand the interplay between the classical properties of the macroscale and the quantum properties of the microscale. This is particularly true in nanomagnetism, where many potential applications require monodisperse, magnetic nanoparticles. One source of such species are single-molecule magnets (SMMs) [1, 2, 3, 4, 5], individual molecules that function as single-domain magnetic particles. Below their blocking temperature, they exhibit magnetization hysteresis, the classical macroscale property of a magnet, as well as quantum tunneling of magnetization (QTM) [6, 7, 8, 9, 10, 11] and quantum phase interference [12, 13], the properties of a microscale entity. QTM is advantageous for some potential applications of SMMs, e.g. in providing the quantum superposition of states for quantum computing [14], but it is a disadvantage in others such as information storage where it would lead to loss of preferential spin alignment. Large SMMs approaching the mesoscale have long been the target of synthesis, and an important question for these (and other mesoscale magnetic particles) is whether they might still unequivocally demonstrate quantum properties, as theoretically predicted [15, 16].

In this letter, we show that a Mn₃₀ molecular cluster is by far the largest SMM to date, and show that it unambiguously still exhibits QTM. This establishes that the quantum physics of the microscale can also be observed in large molecular nanomagnets.

The Mn₃₀ molecular cluster has the formula [Mn₃₀O₂₄(OH)₈(O₂CCH₂CMe₃)₃₂(H₂O)₂(MeNO₂)₄].xCH₂Cl₂.yH₂O and crystallizes in the monoclinic space group C_{2/c} with each Mn₃₀ on a crystallographic C₂ rotation axis [17]. The molecules are thus all parallel

with their molecular C₂ axes (*z* axes) aligned along the crystal *b* axis. Each Mn₃₀ comprises a Mn/O magnetic core (Fig. 1) of volume ≈4 nm³ enveloped in a hydrocarbon shell ≈0.5 nm thick composed of carboxylate CH₂CMe₃ groups. This essentially magnetically isolates neighboring Mn/O cores. However, the large size of Mn₃₀ (volume ≈15 nm³, molar mass ≈6335 Daltons), akin to a small protein, causes inefficient packing in the crystal, with voids between molecules that contain disordered solvent molecules, primarily CH₂Cl₂. In addition, some CMe₃ groups are statically disordered about two sites.

Each Mn₃₀ contains one Mn⁴⁺, twenty-six Mn³⁺ and three Mn²⁺ ions, and exchange coupling between the many spins of the Mn/O core leads to Mn₃₀ having a small net uncompensated spin in the ground state of *S* = 5. The latter was determined from temperature and field magnetization measurements on powdered, microcrystalline samples in the 1.8-4.0 K and 0.1-0.4 T ranges. The data were fit by diagonalization of the spin Hamiltonian matrix assuming only the ground state is populated and incorporating axial anisotropy (*DS_z²*) and Zeeman terms, and employing a full powder average [18]; the Mn₃₀ is thus modelled as a giant spin with Ising-like anisotropy. The corresponding Hamiltonian is given by equation (1):

$$\mathcal{H} = -DS_z^2 + \mathcal{H}_{\text{trans}} + g\mu_B\mu_0\vec{S} \cdot \vec{H} \quad (1)$$

where *D* is the axial anisotropy constant, *S_z* is the *z*-component of the spin operator \vec{S} , $\mathcal{H}_{\text{trans}}$ is the transverse anisotropy, containing *S_x* and *S_y* operators, *g* is the electronic g-factor, μ_B is the Bohr magneton, μ_0 is the vacuum permeability, and \vec{H} is the applied field. The last term in eq. 1 is the Zeeman energy associated with an applied field. The fit parameters were *S* = 5, *D* = -0.73 K, and *g* = 2.00, with the transverse anisotropy $\mathcal{H}_{\text{trans}}$ not included for simplicity (in fact, inclusion of a small transverse anisotropy term involving the transverse

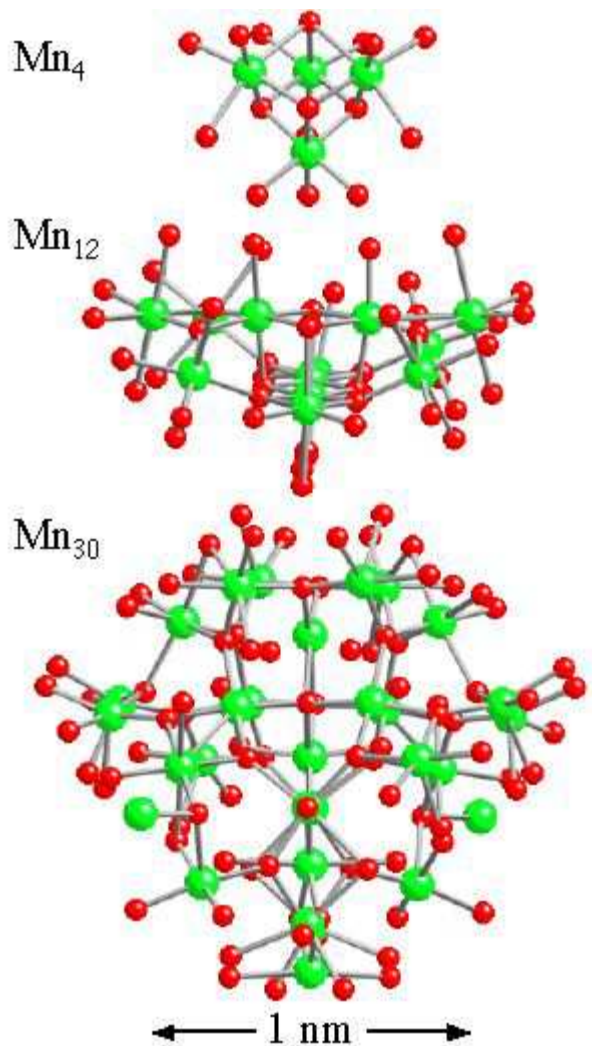


FIG. 1: Schematic view of the Mn/O magnetic core of a Mn₄ [4], Mn₁₂ [5], and Mn₃₀ [17] SMMs. The Mn atoms are depicted larger than the O atoms.

anisotropy constant, E , had no significant effect on the fit). These values suggest an upper limit to the potential energy barrier U to magnetization relaxation (reversal) of $U = S^2|D| = 18$ K, a value potentially large enough to make Mn₃₀ a SMM at sufficiently low temperatures. This was therefore explored by hysteresis loop, relaxation, and hole digging measurements.

Studies were performed on single crystals using an array of micro-SQUIDs [19]. Hysteresis in magnetization versus magnetic field scans was observed, establishing Mn₃₀ as a new SMM, the largest to date. Fig. 2 shows typical hysteresis loops, with the field applied approximately along the easy axis of magnetization. The blocking temperature is about 1.2 K, and the coercivity increases with decreasing temperature and increasing sweep rate, as expected for the superparamagnet-like be-

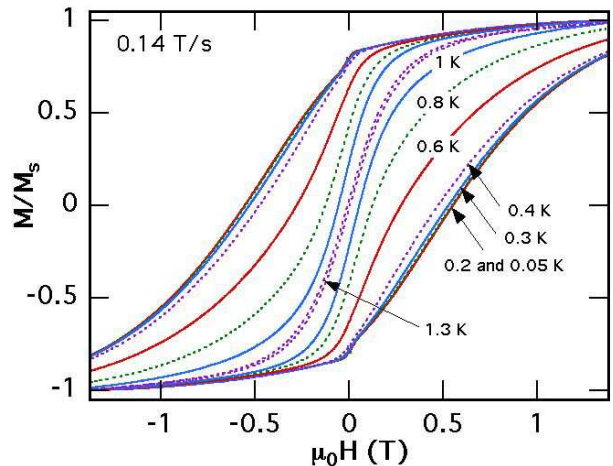


FIG. 2: Normalized magnetization of Mn₃₀ versus applied magnetic field in the 0.05 to 1.0 K temperature range and a field sweep rates of 0.14 T/s. Note that the loops become temperature-independent below about 0.2 K.

havior of a SMM. The loops do not display step-like features characteristic of resonant QTM between the energy states of the Mn₃₀ molecule, as observed for several other SMMs [6, 7, 8, 9, 10, 11, 12]. However, it is possible that steps are present but smeared out by broadening effects due to a distribution of magnetization relaxation barriers (i.e. D values), consistent with the distribution of Mn₃₀ environments resulting from the disordered CMe₃ groups and solvent molecules observed in the crystal structure. It is thus not possible to determine directly from the hysteresis loops whether resonant QTM is occurring in this large Mn₃₀ molecule. Nevertheless, the first indication of quantum tunneling is the temperature independence of the hysteresis loops below about 0.3 K (Fig.2). Detailed measurements of the hysteresis loops show however that the loops are still time-dependent below 0.3 K. This is presented in the inset of Fig. 3 showing the temperature dependence of the coercive field at different field sweep rates. The strong time-dependence in the temperature-independent regime is another important indication of QTM.

QTM can also be confirmed with magnetization decay studies. The magnetization was first saturated at 5 K with a large applied field, the temperature decreased to a chosen value, and then the field removed and the magnetization decay monitored with time. This provided magnetization relaxation rates Γ at different temperatures allowing us to make an Arrhenius plot (Fig. 3) that is based on the Arrhenius law:

$$\Gamma = \Gamma_0 \exp(-U_{\text{eff}}/k_B T) \quad (2)$$

where Γ_0 is the pre-exponential factor, U_{eff} is the mean effective barrier to relaxation, and k_B is the Boltzmann constant. The slope in the thermally activated region

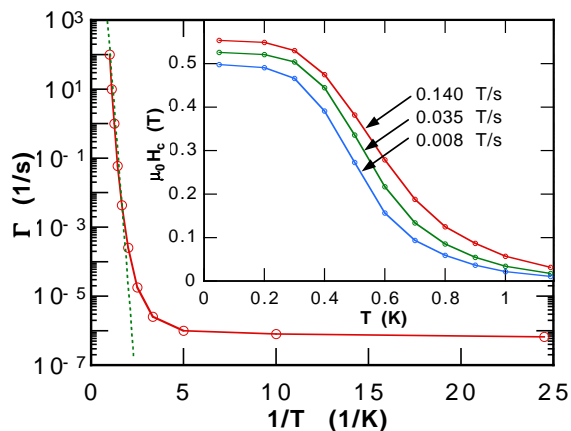


FIG. 3: Arrhenius plot of the relaxation rate Γ versus the inverse temperature for Mn_{30} using data obtained from magnetization decay measurements. The dashed line is the fit of the data in the thermally activated region to the Arrhenius equation; see the text for the fit parameters. Inset: coercive field versus temperature for three field sweep rates.

above 0.5 K gave $U_{\text{eff}}/k_B = 15$ K and $\Gamma_0 = 1.5 \times 10^{-8} \text{ s}^{-1}$. The mean barrier U_{eff} is smaller than the calculated $U = S^2|D| = 18$ K, as expected for QTM between higher energy levels M_s of the $S = 5$ manifold. More importantly, the relaxation time becomes temperature-independent below 0.2 K at about 10^{-6} s^{-1} , diagnostic of ground state QTM between the lowest energy $m = \pm 5$ levels. The crossover temperature between thermally activated relaxation and ground state tunneling is between 0.2 and 0.3 K. The ground state tunneling at < 0.2 K rationalizes the appearance at these temperatures of a QTM step at $H = 0$ in the loops of Fig. 2. Since the tunneling is now only between the lowest m levels, the distribution of Mn_{30} environments no longer has such a large broadening effect on the step at zero field, and a better defined step is seen.

Additional confirmation of QTM in Mn_{30} was obtained from the ‘quantum hole-digging’ method [20, 21, 22, 23, 24]. This is a relatively new method that can, among other things, establish whether resonant tunneling occurs even when steps are absent in hysteresis loops due to a distribution of energy barriers. The method is based on the simple idea that after a rapid field change, the resulting magnetization relaxation at short time periods is directly related to the number of molecules in resonance at the applied field; Prokof’ev and Stamp proposed [20] that this short time relaxation should follow a \sqrt{t} ($t = \text{time}$) relaxation law. Thus, the magnetization of the Mn_{30} molecules in the crystal was first saturated with a large negative field, and then a ‘digging field’ H_{dig} of 0.275 T was applied at 0.04 K for a chosen ‘digging time’ t_{dig} . If QTM can occur in Mn_{30} , then that fraction (and only that fraction) of the molecules that is in resonance

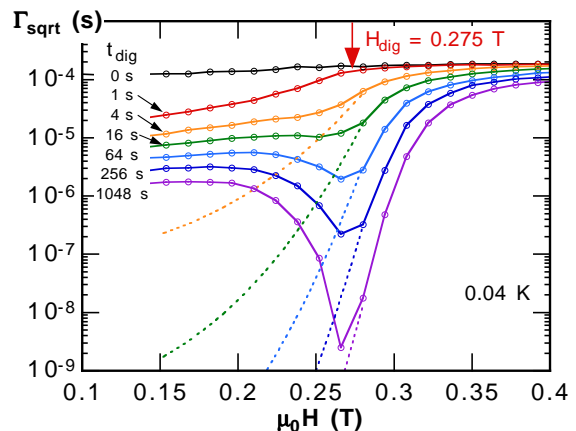


FIG. 4: Relaxation rate at short time periods Γ_{sqrt} versus applied field, determined after application for digging-time t_{dig} of a digging-field H_{dig} of 0.275 T. The sharp dip (‘hole’) at the H_{dig} value shows the depletion of spins that were in resonance at H_{dig} and thus underwent resonant tunneling during t_{dig} . The half-width of the hole of about 20 mT is larger than the hyperfine field (about 10 mT), reflecting the influence of dipolar couplings. A classical system or a quantum system with an continuum of levels would not show a hole but a monotonic increase for $H < H_{\text{dig}}$, indicated schematically by the dotted lines.

at H_{dig} can undergo magnetization tunneling. After t_{dig} , a field H_{probe} is applied and the magnetization relaxation rate is measured for short time periods; from this is calculated the short-time relaxation rate Γ_{sqrt} , which is related to the number of Mn_{30} molecules still available for QTM [19]. The entire procedure is then repeated at other H_{probe} fields. The resulting plot of Γ_{sqrt} versus H_{probe} reflects the distribution of spins still available for tunneling after t_{dig} , and it will display a ‘hole’ if resonant QTM did indeed occur during application of H_{dig} for time t_{dig} . The obtained plot for Mn_{30} (Fig. 4) does show a hole in this distribution, corresponding to a depletion of those spins that were in resonance and able to tunnel during t_{dig} at H_{dig} . The occurrence of resonant QTM in Mn_{30} is thus confirmed, since a classical system or a quantum system with an continuum of levels will not show a ‘quantum hole’ but rather a depletion of all spins with low barriers (Fig. 4).

The above results unambiguously demonstrate that Mn_{30} undergoes tunneling, involving the coherent reversal of about 600 interacting electron spins within the Mn/O magnetic core. Of the three diagnostic tests for resonant QTM, Mn_{30} clearly demonstrates two of them, temperature-independent relaxation and quantum hole digging. The third is steps in hysteresis loops, but these are broadened beyond resolution by the distribution of barriers (D values) resulting from a distribution of Mn_{30} environments. Mn_{30} thus represents the largest SMM by far to unequivocally demonstrate QTM, establishing

that quantum effects can be clearly observed, and studied, even in very large 'magnetic particles' with dimensions approaching the mesoscale. This is made possible in Mn_{30} by its monodisperse nature and highly ordered arrangement within the crystal (notwithstanding the solvent and CMe_3 disorder, which in an absolute sense is a small perturbation), which prevent complications from distributions of particle size, shape, surface roughness, and spin. The latter have severely hampered previous attempts to demonstrate QTM in large magnetic particles, both for classical magnetic materials such as Co metal and molecules such as the ferritin protein. The results have consequently usually been negative, unclear or controversial [25, 26, 27, 28, 29]. In contrast, the present work demonstrates that crystalline assemblies of monodisperse molecular nanomagnets allow clear observation of quantum properties under straightforward conditions even for large systems approaching the mesoscale, the hydrocarbon shell of organic groups in Mn_{30} ensuring the Mn/O cores are exactly identical in every molecule.

From a broader point of view, the present work confirms that large SMMs can be prepared and studied as crystalline assemblies of monodisperse particles. Mn_{30} is much bigger than other currently known SMMs such as Mn_4 , Mn_{12} , etc, and thus represents proof-of-feasibility of extending to larger species the many advantages of SMMs over classical magnetic particles. These include monodispersity, crystalline order, room-temperature solution synthesis, true solubility (rather than colloidal suspension) in common organic solvents, and an insulating shell of organic groups around the magnetic core, which additionally can be varied at will using standard synthetic chemistry methods. Such factors are clear benefits for the many proposed applications of SMMs, for example as qubits in quantum computing [14], where the larger is an individual SMM, the easier it should be to manipulate and measure its quantum state. The synthetic variation of the hydrocarbon shell can also provide a facile way to increase (or decrease, if desired [30]) the isolation of a single SMM from its neighbors, and perhaps thus also help decrease decoherence problems.

We thank the USA National Science Foundation for support.

-
- [1] G. Christou, D. Gatteschi, D.N. Hendrickson, and R. Sessoli, *MRS Bulletin* **25**, 66 (2000).
 [2] R. Sessoli, H.-L. Tsai, A. R. Schake, S. Wang, J. B. Vincent, K. Folting, D. Gatteschi, G. Christou, and D. N.

- Hendrickson, *J. Am. Chem. Soc.* **115**, 1804 (1993).
 [3] R. Sessoli, D. Gatteschi, A. Caneschi, and M. A. Novak, *Nature* **365**, 141 (1993).
 [4] S. M. J. Aubin and *et al.*, *J. Am. Chem. Soc.* **118**, 7746 (1996).
 [5] C. Boskovic and *et al.*, *J. Am. Chem. Soc.* **124**, 3725 (2002).
 [6] J. R. Friedman, M. P. Sarachik, J. Tejada, and R. Ziolo, *Phys. Rev. Lett.* **76**, 3830 (1996).
 [7] L. Thomas, F. Lioni, R. Ballou, D. Gatteschi, R. Sessoli, and B. Barbara, *Nature (London)* **383**, 145 (1996).
 [8] C. Sangregorio, T. Ohm, C. Paulsen, R. Sessoli, and D. Gatteschi, *Phys. Rev. Lett.* **78**, 4645 (1997).
 [9] S. M. J. Aubin, N. R. Dilley, M. B. Wemple, G. Christou, and D. N. Hendrickson, *J. Am. Chem. Soc.* **120**, 839 (1998).
 [10] S. M. J. Aubin, N. R. Dilley, M. B. Wemple, G. Christou, and D. N. Hendrickson, *J. Am. Chem. Soc.* **120**, 4991 (1998).
 [11] C. Boskovic, M. Pink, J.C. Huffman, D. N. Hendrickson, and G. Christou, *J. Am. Chem. Soc.* **123**, 9914 (2001).
 [12] W. Wernsdorfer and R. Sessoli, *Science* **284**, 133 (1999).
 [13] A. Garg, *EuroPhys. Lett.* **22**, 205 (1993).
 [14] M. N. Leuenberger and D. Loss, *Nature* **410**, 789 (2001).
 [15] E. M. Chudnovsky and L. Gunther, *Phys. Rev. Lett.* **60**, 661 (1988).
 [16] B. Barbara and E.M. Chudnovsky, *Phys. Lett. A* **145**, 205 (1990).
 [17] M. Soler, E. Rumberger, K. Folting, D. N. Hendrickson, and G. Christou, *Polyhedron* **20**, 1365 (2001).
 [18] J. Yoo and *et al.*, *Inorg. Chem.* **40**, 4604 (2001).
 [19] W. Wernsdorfer, *Adv. Chem. Phys.* **118**, 99 (2001).
 [20] N.V. Prokof'ev and P.C.E. Stamp, *Phys. Rev. Lett.* **80**, 5794 (1998).
 [21] W. Wernsdorfer, T. Ohm, C. Sangregorio, R. Sessoli, D. Mailly, and C. Paulsen, *Phys. Rev. Lett.* **82**, 3903 (1999).
 [22] W. Wernsdorfer, A. Caneschi, R. Sessoli, D. Gatteschi, A. Cornia, V. Villar, and C. Paulsen, *Phys. Rev. Lett.* **84**, 2965 (2000).
 [23] J. J. Alonso and J. F. Fernandez, *Phys. Rev. Lett.* **87**, 097205 (2001).
 [24] I. Tupitsyn and P.C.E. Stamp, *cond-mat/0305371* **5**, 5371 (2003).
 [25] D. D. Awschalom, J. F. Smyth, G. Grinstein, D. P. DiVincenzo, and D. Loss, *Phys. Rev. Lett.* **68**, 3092 (1992).
 [26] S. Gider, D. D. Awschalom, T. Douglas, S. Mann, and M. Chaparala, *Science* **268**, 77 (1995).
 [27] J. Tejada and *et al.*, *Science* **272**, 424 (1996).
 [28] H. Mamiya, I. Nakatani, and T. Furubayashi, *Phys. Rev. Lett.* **88**, 067202 (2002).
 [29] W. Wernsdorfer, E. Bonet Orozco, K. Hasselbach, A. Benoit, D. Mailly, O. Kubo, H. Nakano, and B. Barbara, *Phys. Rev. Lett.* **79**, 4014 (1997).
 [30] W. Wernsdorfer, N. Aliaga-Alcalde, D.N. Hendrickson, and G. Christou, *Nature* **416**, 406 (2002).